Journal of Energy Challenges and Mechanics
http://www.nscj.co.uk/JECM/
ISSN 2056-9386
Volume 1 (2014) issue 3, article 7

Effect of PV module frame boundaries on cell stresses in solar cells

光伏模块的框架边界对太阳能电池板中应力的影响

Johannes Schicker[1*], Christina Hirschl[1], Roman Leidl[2]

[1] *CTR Carinthian Tech Research AG, Europastraße 4/1, 9524 Villach, Austria*
[2]*AIT Austrian Institute of Technology, A-1220 Vienna, Austria*

johannes.schicker@ctr.at

Accepted for publication on 15th November 2014

Abstract - **Usually, stresses in module integrated solar cells are obtained by Finite Element (FE) calculations because these stresses can hardly be determined by measurements. Apart from the knowledge of the material properties, the FE boundary conditions have a distinct effect on the results of a FE solution for a standard mechanical pressure test. We used different simplified approximations to the complex real clamping of pv modules for simulating the deformation of the module and hence the stress-strain situation in the cells. Some deformation results could be compared to experimental findings from a standard mechanical load test. In this paper we show the bandwidth of results from variations of the assumptions which were made for the simulations. We found that particularly weak modules, i.e. thin frame and thin glass plate, show a strong dependency of cell stresses on the boundary conditions of the FE model. Hereby, the calculated stresses resulting from one assumption can easily deviate for more than 50% from the stresses using another assumption, even when the displacements are nearly equal and both lie closely to the measured values. Finally, we outline one possibility to directly in situ measure the cell strains what could help to resolve this uncertainty.**

Keywords – **Solar cells, mechanical stresses, standard load test, Finite Elements, boundary conditions.**

关键词 – **太阳能电池, 机械应力, 标准加载实验, 有限单元法, 边界条件。**

I. INTRODUCTION

The key to long term operating stability of photovoltaic (pv) modules is the integrity of the solar cells. One of the main factors responsible for the loss of cell integrity in outdoor modules are mechanical stresses due to external loads, as e.g. snow, imposed on the module. A good estimate of the arising mechanical stresses is a crucial prerequisite to estimate the fracture probability of a silicon solar cell. For a module design it is also desirable to determine the stresses in advance without time and cost extensive experiments. But even for already existing modules, due to the inaccessibility of the cells inside the module, it is hardly possible to measure the cell stresses during load application in a standard mechanical load test. Finally, the stresses are usually obtained by simulations using Finite Element (FE) analyses**.**

A primary component of a realistic model is an adequate constitutive model for the materials of the pv laminate and its corresponding parameters. Aside from the laminates response to external loads, also its mounting and clamping has a distinct effect on the module's behaviour. The mounting of the laminate is usually realised by a metal frame which itself is clamped onto a metal base frame. Both are subjected to deformations. The complex clamping is hardly transferable into Finite Element boundary conditions. Hence, some simplifying assumptions must be made. The simplest boundary condition of the laminate results from the idealisation of the frame as rigid. Then the laminate can be regarded as fixed at all edges, and either it may rotate freely about the edges or it is fully restrained, depending on the character of the fitting of the laminate in the frame. Implementing into the model the ability of the frame to bend under load adds an additional level of complexity. And finally, this complexity is added for the base frame, too.

Three different types of commercial pv modules were investigated. On one hand they were subjected to a mechanical load test according to international standards (IEC 61215 sub clause 10.16) in the test facilities of AIT, while on the other hand these tests were simulated at CTR using Finite Element analyses. From the experiments the deflections at some designated points of the modules were obtained and served for calibration of the calculations. Aim of the simulations was to determine the cell stresses that arise in the modules.

The frame geometries of the modules were obtained from the manufacturers as CAD data. The laminate thicknesses (glass, EVA, cells, back sheet) were also known. The characteristics of the module clamping in the test stand had to be simplified for the simulation but still should describe the bonding condition of the test situation close enough to match the actual module behaviour. This led to a systematic study how the boundary conditions of the FE model affect the

module's overall behaviour, i.e. the deformations, and the cell stress in particular.

II. Module Properties

We chose three different types of pv modules for testing and modelling. They differed in size, material of the back sheet, thickness of the glass, and in the frame geometries. All frames were built of the soft aluminium alloy AlMgSi-T66. We approximated its stiffness behaviour using a bilinear hardening elastic-plastic constitutive law, whereas the geometries were taken as detailed as necessary. All cells were 156x156 mm multi crystalline solar cells with a thickness of 180 µm. We used an isotropic elastic material law for them as proposed by Hopcroft [1]. They were encapsulated by 360 µm EVA on each side. We assumed the EVA to be strain- and stress-free in the unloaded module. Although EVA is known to behave visco-elastic (see e.g. [2]), we applied a linear elastic behaviour using an initial short term stiffness as we considered the duration of the load tests as comparably short. This stiffness, however, is not known; and we found contradictory values. From a manufacturer we found a Young's modulus of 65 MPa, [3], but we doubt this to be valid for cross linked EVA. Another value was estimated by polymer experts assuming rather something about 10 MPa. For this study we used 65 MPa in the first place for all simulations, but then, we varied this stiffness in additional simulations, were we used both 6 and 0.6 MPa instead for the otherwise identical models, and compared the results. To model the sealant between laminate and frame we supposed soft sanitary silicon with an elastic behaviour with a Young's modulus of 15 MPa. All calculations were done using large deformation theory and postulated double symmetry.

Module type #1 was a 54 cell module with 3.2 mm front glass and a lean and low built frame, whereas module types #2 and #3 had 60 cells and higher and stiffer frames. Module type #2 had 4 mm front glass and module type #3 again had a 3.2 mm thick front glass. The back sheet of module types #1 and #2 was a standard TPT foil (a Tedlar/PET/Tedlar composite), whereas module type #3 had a pure polyamide foil (Icosolar® AAA 3554, Isovoltaic AG). The TPT foil is stiffer than the polyamide AAA foil, a Young's modulus of 1.3 GPa and 5 GPa, respectively, can be assumed. Furthermore, the cavity in the frame where the laminate is to be fitted in varied between the frames. It was higher and less deep in the frame of module type #2 than in the two others. The free height after inserting the laminate in module #2 was 2 times 775 µm, whereas in type #1 only 2 times 150 µm, and in module type #3 2 times 225 µm were filled with sealant. In contrast the embedment depth of the laminate was only 5 mm into the cavity of the frame type #2, whereas it was 10.5 mm into the frame of module #1, and 11.3 mm into frame #3. Fig. 1 shows the three frames in their respective relative size and the embedment of the laminates.

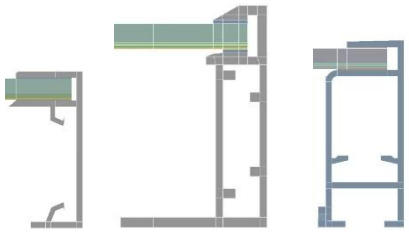

Fig.1, Sketches of module frames and their respective relative sizes. From left: module types #1, #2, and #3.

In all simulations a uniform pressure load onto the glass of the module was applied. For comparability, we only applied the lowest load that was not disturbed by secondary effects in any of the modules. This load was 2400 Pa, since the backside of module #1 was pressed against the base frame at a pressure just above 2400 Pa, see Fig. 2. In addition, the frame of module type #1 showed plastic yielding next to the mounting point at higher loading, whereas both other frames still behaved elastically at this load.

Fig.2, At a load higher than 2400 Pa the back sheet of module type #1 is pressed onto the supporting beam.

III Mounting System of PV Laminates and FE Boundary Conditions

Industry provides different mounting systems for solar modules. Most consist of a base frame of metallic beams with a second frame of beams mounted crossways on the first beam layer. Then, the module's frame is clamped onto these upper bars. The laminate of glass, solar cells, encapsulant, and back sheet was already inserted in the frame cavities and sealed and fixed by soft silicon at delivery of the module.

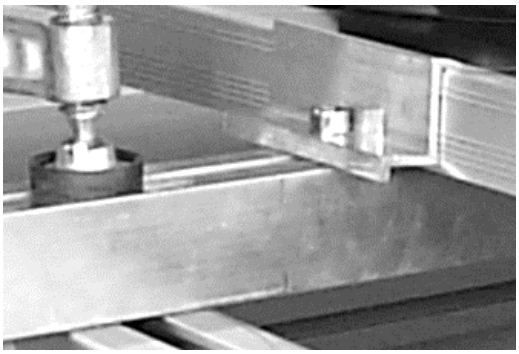

Fig.3, Clamping of the frame to the supporting beam and of the beam to the base frame.

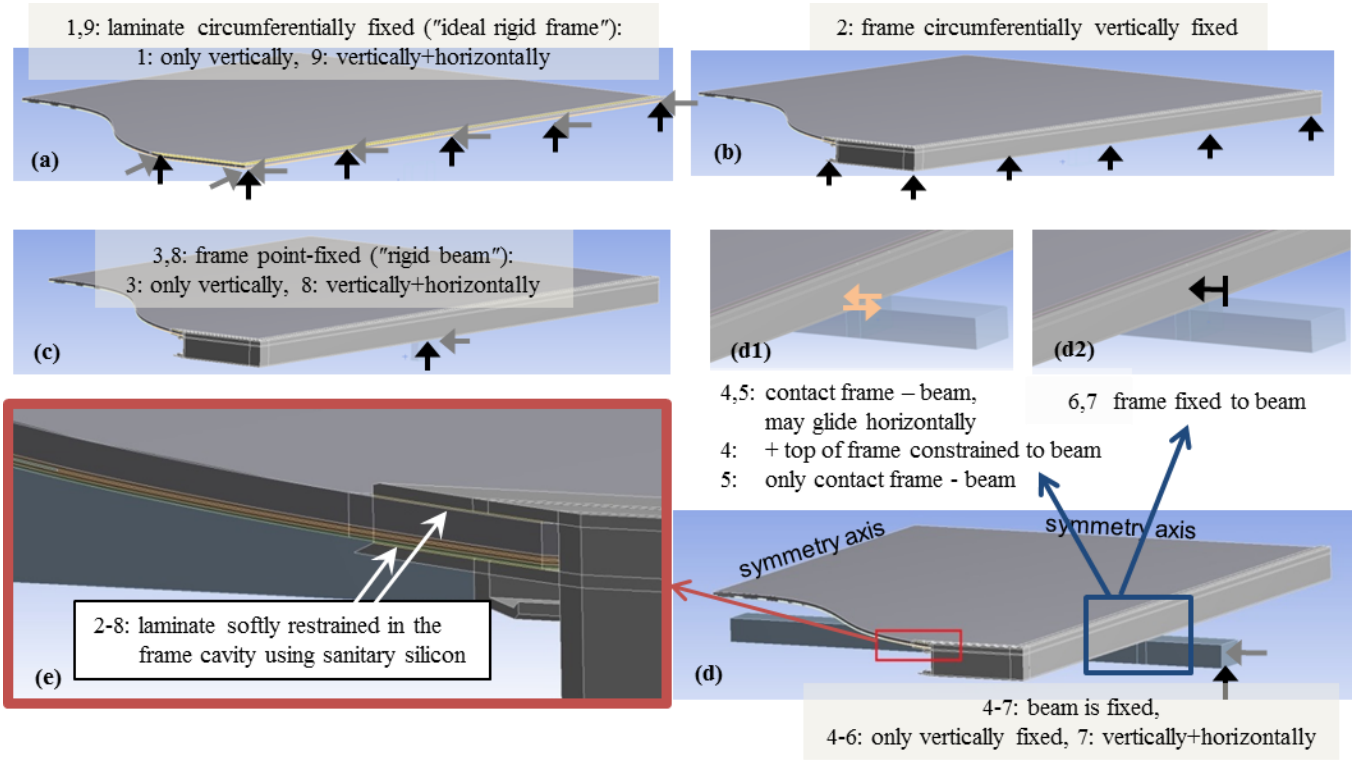

Fig.4, Laminate bonding conditions: (a) Models 1 and 9: pure laminate bonded circumferentially, (e): in all other models, i.e. 2-8, the laminate is restrained in its respective frame. (b) shows a circumferentially fixed frame, (c) shows a frame that is fixed in space at its supporting point to the beam, (d) shows the frame on its supporting beam where the protruding end of the beam is fixed. (d1) and (d2) symbolise the beam-frame interaction of model (d), i.e. models 4-7. The lighter, horizontal arrows in (a), (c) and (d) are active restraints only in the models

The mounting system used during the laboratory tests is designed to emulate a customary mounting system. It consists of an almost rigid base frame, a pair of standard profiled aluminium beams used in pv applications is screwed to this base frame and the module is clamped to the profiled bars. For clamping, a S-shaped piece of aluminium presses the top face of the module frame down so that the frame's lower surface has frictional contact to the profiled bar, see Fig. 3.

The attempt of modelling this scenario in a Finite Element analysis revealed several unexpected difficulties and disadvantages. First of all, the requirement for modelling several separated contact problems increases the calculation costs immensely. Then, without knowledge of the pre stress of the clamps, it can not be expected to get realistic results. Therefore, we began with a simple approximation to the real mounting situation and successively refined it. In the following we use the term "model" to address the different refinements of the FE assumptions for the module bonding problem. Fig. 4 sketches the following explanations.

For the laminate bonding we used two general refinements in the Finite Element simulations: first, the pure laminate was bonded circumferentially at its edges, addressed as **model 1**, see Fig. 4(a), and second, the laminate was softly restrained in the cavity of its frame by entirely filling the gap between the laminate's surfaces and the frame with 2 layers of soft sanitary silicon, Fig. 4(e). The following models, except model 9, base on the latter and only the kind of bonding of the frame is varied. Obviously, bonding the laminate without a frame is just a fictitious construct and model 1 just serves for the purpose of comparison as representation for an infinite stiff frame.

The simplest assumption for the frame bond is to circumferentially fix the frame's bottom faces in space. This varies the idea of a stiff frame but the frame may twist when the off-centred laminate is loaded. This is addressed as **model 2**, see Fig. 4(b). The next model, **model 3**, represents a frame on a rigid beam. Here, the frame is only fixed in space where it is supported by the beam whereas the remaining lower surface of the frame stays unsupported, Fig. 4(c). In a further refinement step, we also modelled a flexible supporting beam that protrudes from the module frame by about 90 mm before it is supported by the base construction, compare Fig. 3. The beam is only fixed at the protruding end where it is supported by the base frame, Fig. 4(d). The module frame is then fixed on the beam, Figures 4(d1) and (d2). In this constellation, the module frame may be displaced as a whole when the module is pressed down and the beam is bent. But in addition, the module may also be twisted at contact to the deformed support. In **Model 4** the top of the frame is constrained to the bar by using a constraint equation to simulate the clamp. The contact between the bottom of the frame and the supporting beam was assumed to be frictionless. This model was modified by **model 5**, in which we removed the constraint equation for better convergence of the calculation and only the pressure contact remained.

Models 1 to 5 have in common, that only the vertical directions are fixed, whereas the horizontal movements of the

module are restrained by symmetry conditions for the module. Accordingly, the frame boundary conditions allow for a horizontal movement along the beam axis of the frame bond when the module becomes bent. This horizontal movement is small but increases with the height of the frame. The real clamping, however, restrains this movement partially by friction. To check the influence of this mobility, some models where added that also restrain the horizontal movement where the frame is supported. **Model 6** is the variation of model 5 in which the contact area between beam and frame is replaced by common nodes. **Model 7** adds to model 6 a horizontal restraint at the contact area between supporting beam and base construction. **Model 8** corresponds to model 3, i.e. a small part of the frame's lower surface is now totally fixed in space. Finally we applied a total horizontal constraint to the pure laminate edges, i.e. we modified model 1 to **model 9**. In Fig. 4(a), (c) and (d) lighter arrows mark these additional constraints. There is also a **model 10**, which is a modification of model 9 for cross-checking the results. It will be explained later.

Only the first 6 models were applied to all three module types. The models 7 and 8 were only tested with the weak module type #1. Model 9 was only used as comparison to model 1, and, since in both models no frame is involved, one calculation seemed sufficient. This was done with the laminate of module type #3, for which also model 10 was adapted.

The supporting beam in the tests was a thin walled profiled bar. Instead of modelling it in detail, we tested the elastic deformation vs. force of the beam separately. In the simulations we then substituted it by a massive bar with the same elastic behaviour.

IV. Simulation Results

The most obvious difference of the module behaviour for different bonding conditions can be seen in Figures 5 and 6. Here the deformations are shown for the models 1 and 3, resp., i.e. an ideal rigid frame and a flexible frame bonded only at the contact point to the supporting beam. Both figures use an identical colour translation to the size of the module deflections. Due to the deformation of the frame the deflection in the centre of the module for model 3 is about twice as high as for model 1.

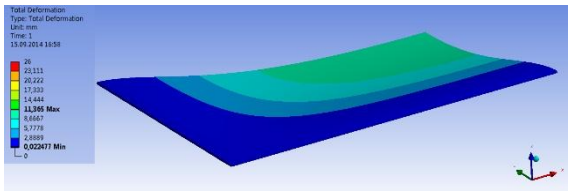

Fig.5, Total deformation of model 1 (¼ module)

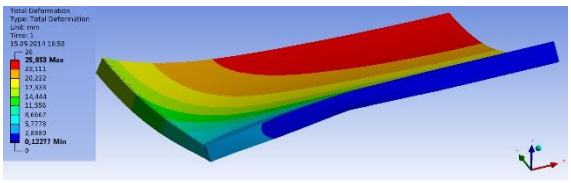

Fig.6, Total deformation of model 3 (¼ module)

The deformation of model 3 as it is shown in Fig. 6 is in good agreement with the observed deformation of the frame and module. In general, all calculations assuming a flexible module frame that is punctually supported agree with the behaviour of the tested modules, i.e. the frame buckles where it is punctually supported, and the outer frame part is deeper than the middle part. The absolute displacement values of the tested modules, however, were not achieved due to the fact that all of the simulations display slight stiffer module behaviour than the test modules. The displacement measurements, however, scattered widely from module to module even for the same module type. As most likely reason we identified the corner joint of the modules, which is not as monolithic as modelled. In the real modules, the corner joints are stuck together and the joint is movable to some extend. The scatter of the measured deformations is higher than the differences between the calculated values of all models of one module type. From comparing the measured module displacements it can therefore not be decided which model is best suited to approximate the real clamping situation. Only clear is that models 1 and 2 violate the basic deformation criteria of the clamped real modules.

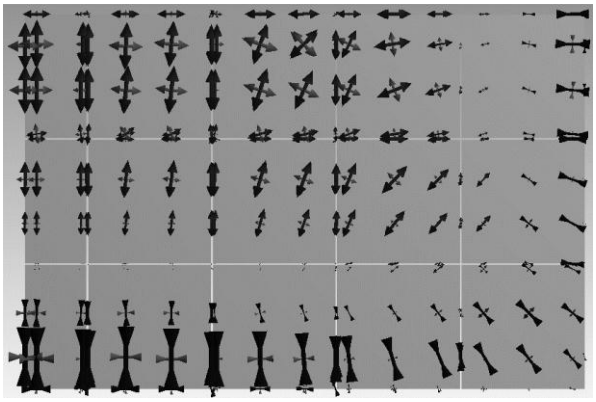

Fig. 7; Directions of the principal stresses from model 1, i.e. of a pure laminate panel circular bonded normal to the panel plane, calculated at 2400 Pa pressure. The symmetry planes are on the left and upper side, resp.; the bonded sides are right and at the bottom.

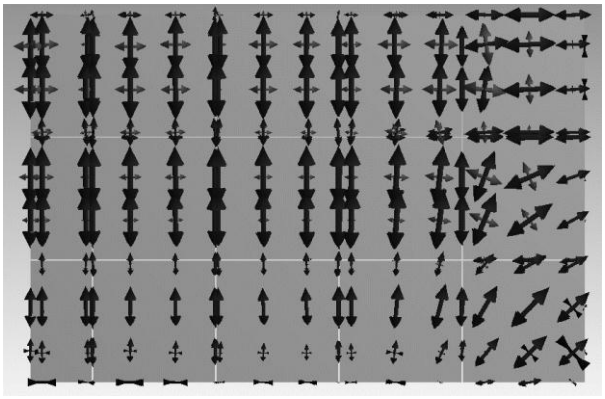

Fig.8: Directions of the principal stresses from model 3. i.e. a laminate panel fixed in its frame and the frame bonded at the position of the supporting beam, calculated at 2400 Pa pressure. The symmetry planes are on the left and upper side, resp.; the framed sides are right and at the bottom.

Figures 7 and 8 show the directions of the calculated principal stresses on the bottom side of the cells for model 1 and 3, respectively. The position of the supporting beam and a numbering convention for the cells can be seen in Fig. 9. It also shows schematics of the two different types of module-dimensions, a 54 cell module and a 60 cell module, viewed from below. The drawing shows modelled quarters of the double symmetric modules with the supporting beams.

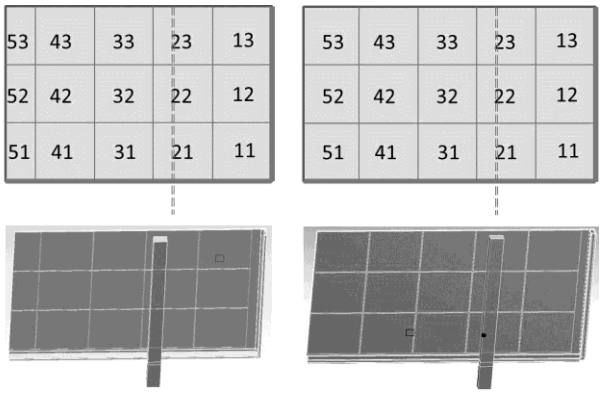

Fig.9, Cell numbering of the quarter modules, viewed from below, and position of the supporting beam: left a module with 54 cells, right a module with 60 cells.

The assumption of a rigid frame as it is represented by model 1 leads to pressure stresses (inverted arrows) along the supported laminate, see Fig. 7, with their maximum direction normal to the edges. But, considering a punctually supported flexible frame as in model 3, see Fig. 8, leads predominantly to tensile stresses (outward arrows). Furthermore, the direction of the principal stresses changes abruptly after the first column of cells. Inside the module part between the supporting points all arrows go parallel to the shorter frame side. In all the models 3 to 8 the principal stresses in cell 11 are tensile stresses having an angle of approximately 45° against the frame, whereas in cell 13 the maximum principle stresses are parallel to the longer module edges. The bus bars, which were not modelled, should go along the longer module edges, whereas the steeper deflection goes perpendicular to the bus bars direction. The maximum principle (tensile) stresses in the centre of the module are orientated in this direction.

The stresses in the test modules could not be determined, but electroluminescence pictures of modules with broken cells after cycles of loading and unloading were taken. The cells are fracturing brittle and most theories postulate that brittle fracture is due to the maximum tensile stresses, where cell breakage usually occurs normal to the direction of the maximum tensile stress. In the test modules we observed a crack pattern that is in agreement with the orientation of the maximum principal stresses of Fig. 8 of the punctually supported module, i.e. we found cracks in the corner cells under an angle of 45° and in cell number 21 under an angle of approximately 20° against the longer frame side.

To compare the different models to each other, we focus on the maximum principal stresses in three cells. Nearly all simulation models of all three module types show the highest principle stress values in cell 53 or sometimes in cell 22. In very few calculations the highest value can be found in cell 43, but then, the value is only insignificant higher than in cell 53. The corner cell, number 11, is of interest because of its pronounced 45° direction of the principal stresses. In the Figures 10 to 12 the maximum principle stresses in these three cells are compared for all variations of the FE boundary conditions we applied to the three module types. The massive bullets, corresponding to the right y-axes of the graphs, show the corrected deflection values in the module centre for comparison. The corrected deflection value is obtained by subtracting the vertical displacement of the frame at its fixing point from the vertical displacement in the module centre. The stress values are all evaluated in the centre of the respective cells, although specifically in cell 11 and cell 22 sometimes the highest values were not found in the middle of the cell. For the benefit of legibility the scales of the axes differ in the diagrams.

In Fig. 10 for module type #1 a strong dependency of the overall stress level and module deflections on the boundary conditions in the Finite Element analysis can be seen. The general picture of the simulation shows that the module deflection and the stress levels are increasing when the number of restraints decreases. The least deflection corresponds to the least stresses if only the pure laminate is considered, model 1. The highest deflection yields the highest stress level with model 5, where we included the supporting beam as a deformable component and allowed both the frame and the beam to move along the beam axis. This movement, however, was very small and hardly noticeable by the eye. The horizontal movement was calculated to be 1.4 mm for the frame and 0.14 mm for the beam. Comparison of models 6 and 7 with model 5 shows that the most important constraint is the constraint of the frame to the beam in model 6, whereas the constraint of the beam itself is not adding much effect. Both restraints yield about the same effect as a vertical restraint at the mounting point of the frame, model 3. Only model 8, where the frame's mounting point is fully fixed in space, shows a

further significant decrease of deflection and stress level, but it still does not reach the smaller values calculated for the unbending frame of the models 1 and 2.

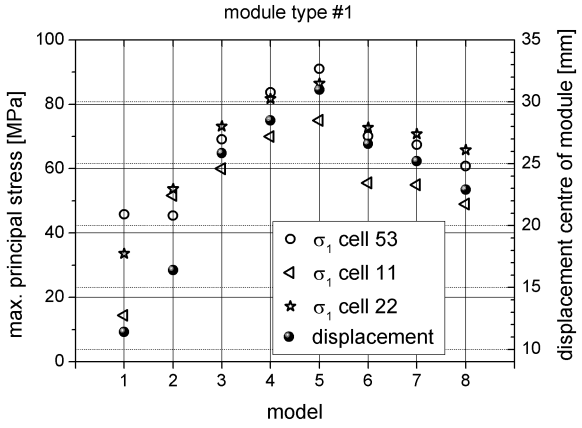

Fig.10, Stresses and deflections in dependency of various Finite Element boundary conditions for module type #1.

Considering the larger module type #2 we observe a very similar dependency, namely an increasing stress and deflection level with the decrease of restraints, see Fig. 11; only model 1 does not fit in the picture. Here, the deformation becomes smaller when adding a frame, model 2 corresponds to the framed model 1. The explanation can be found in the stiff frame of module type #2. Here, the pure laminate is stiffened by the frame, whereas the soft frame of module type #1 adds additional flexibility.

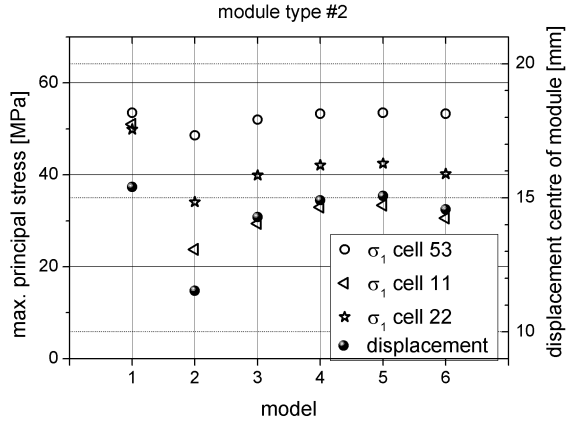

Fig.11, Stresses and deflections in dependency of various Finite Element boundary conditions for module type #2

Another observation for the stiffer module can be made: in Fig. 10 for module type #1 the stresses in cell 22 are nearly as high as the stresses in the centre cell number 53 and even higher in some boundary models. Module type #2 has a pronounced ranking of stresses: The stress in the centre cell is always significant larger than the stress in cell 22 and this itself has a pronounced larger value than cell 11. Only the frameless model 1 shows a higher value in cell 11 than in cell 22. Since there was not much difference in the results of models 6, 7, and 8, at the weak module type #1, calculation of models 7 and 8 had been omitted for this module type. However, it can be seen in Fig. 11 that the stiff module leads to the comfortable situation that neither of the punctual support models 3 to 6 yields much difference, neither in the deflections of the centre of the module nor concerning the stresses.

Module type #3 is also a large module, i.e. 60 cells, with a stiff frame that is comparable to frame #2, but with the same glass thickness (3.2 mm) as module #1. In this module, the frame adds stiffness to the pure unframed laminate as already observed in module type #2, compare models 1 and 2 in Fig. 12. But different from module #2, in module type #3 the stiffness of the frame only reduces the cell stress in the corner cell number 11, whereas the stress in cell 22 increases from model 1 to model 2 and the stress in cell 53 only decreases slightly. We conclude this to be an effect of the thinner glass: the frame stiffens only the adjacent part of the laminate. Thus, the reduced displacement in the centre of the module is a result of the shorter distance in which the laminate is bent.

As in the other modules the cell stresses and module deflections increase with the number of bonds that are unrestrained. Here, we added model 9 to the simulations to verify this trend. Model 9 is a pure laminate without frame, but instead of bonding the edges only vertically, as in model 1, they are restrained horizontally, too. It can easily be noticed, that both, the vertical displacement of the module centre and all stresses decrease from model 1 to model 9.

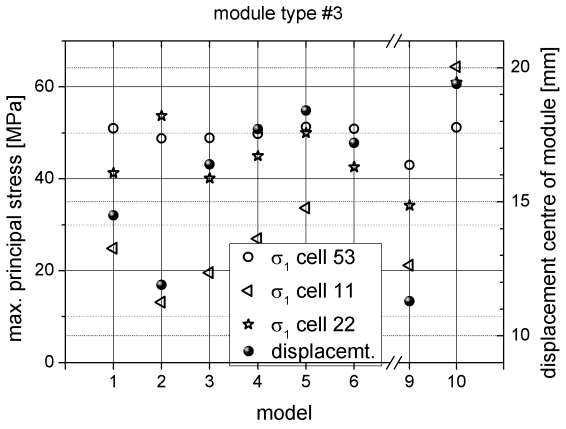

Fig. 12: Stresses and deflections in dependency of various Finite Element boundary conditions for module type #3

Finally we wondered why the pure laminate of module type #3 has approximately the same deflection and cell stress as the laminate of module #2 although it has a much thinner glass. After close examination we realised, that the embedment depth into the frame was different: module type #3 is 11.3 mm deep embedded into the frame whereas module type #2 has only 5 mm depth. When bonding the pure laminate, we used the embedment depth for applying the edge bonding, i.e. we fixed the vertical displacements of the laminate in the area where the laminate is embedded in the frame. To check, that the reason for an approximate equal deflection in both laminates, i.e. that

with the thinner glass and that with the thicker glass, is the different depth of bedding we implied **model 10**, an artificial boundary condition, where we reduced the area of constraint of module type #3. Model 10 has now the same embedment depth of 5 mm as model 1 in module type #2 has. As expected, now, the model with with reduced depth of bedding, model 10, has a much higher deflection and also higher cell stresses than model 1 of the same module type. Now, the comparison of pure laminates between the thinner glass, module type #3, and the thicker glass, module type #2, meets the expectation.

V. Influence of the EVA Stiffness

Until this point, we calculated all results using a rather high value for the EVA stiffness. This value was an arbitrary choice when we started these simulations, and was maintained for the sake of comparison. Now, we examine the question whether the principle statements we found still hold if the EVA stiffness is significantly different from the assumed value.

It is obvious that the module deflections depend on the EVA stiffness, because without EVA only the glass would contribute to the bending stiffness of the laminate. A very weak EVA can not transmit much force to the cells and hence their stresses tend to zero. On the other hand, a very stiff EVA transmits bending forces to the cells which are located in the tensile zone of the composite plate and, hence, the cells can contribute to the bending stiffness of the laminate. Therefore, the cell stress must depend on the EVA stiffness.

We applied different values of the EVA stiffness to the models 3 and 5 of the precedent simulations of module type #1, without changing anything else. The results are depicted in Fig. 13.

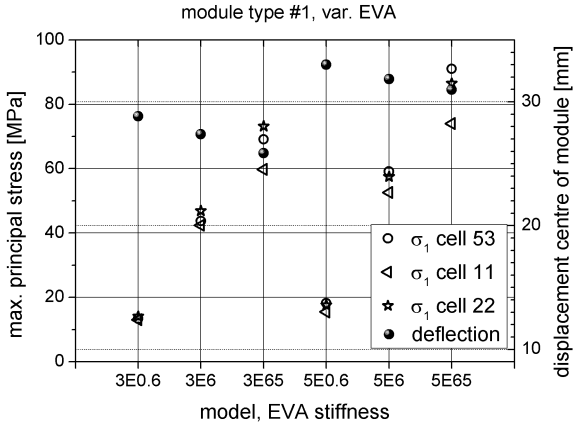

Fig.13, Dependency of module deflection and cell stress on the stiffness of EVA for otherwise identical simulation models: left in the drawing are shown results for model 3 using an EVA stiffness of 0.6, 6.0, and 65.0 MPa, and right in the drawing are shown the results using model 5.

We named the models 3E0.6, 3E6, and 3E65 to express model number 3 with EVA stiffness 0.6 MPa, 6 MPa, and 65 MPa, respectively, and 5E0.6, 5E6, and 5E65 for model 5 with EVA stiffness 0.6 MPa, 6 MPa, and 65 MPa, respectively. With stiffness the Young modulus is meant. Clearly, 3E65 and 5E65 are already shown in Fig. 10. As it can be seen, the deflections of the modules become larger and the cell stresses decrease with decreasing stiffness of the EVA. The displacements and stresses of model 5 are higher than those of model 3 for each equal EVA stiffness. The stress values in the different cells approach each other and tend to zero with decreasing EVA stiffness. We conclude, that the previous findings stay valid for all stiffnesses of EVA, namely that with increasing number of unrestrained module bonds the cell stresses and module deflections increase

VI. About in situ Measurement of Cell Strains

We have shown that the stresses of the solar cells in pressure loaded modules depend on various factors. Even with good knowledge of the true behaviour of EVA uncertainties remain concerning the true frame behaviour and the appropriate boundary conditions in a FE analysis to obtain a good estimation of the resulting cell stresses. Measuring these stresses directly in situ at the strained cells seems inevitable to validate the simulation results. Our expectation is that this can be achieved using strain sensors that are applied to the rear faces of the cells. The solar cells are very thin and normal pressure loading conditions on modules lead basically to stress states in the cell plane. Hence, a plane stress state is a reasonable proper assumption. Further on, since the cell strains of undamaged silicon are considered to be small, a linear Hook's stress strain constitutive law for the cells can be assumed so that stresses and strains can interchangeably be considered. This justifies the suitability of in-plane strain sensors for monitoring cell stresses.

We suggest attaching 45° strain gauge rosette micro-strain sensors (RY89-3/350, HBM GmbH) to the backside of the respective cells. These sensors consist of three independent strain gauges to capture the normal elongations in three coplanar directions of a field of about 5x5 mm. From these data the three independent components of a plane strain tensor can be determined. Electrically, each sensor leg has to be part of a full Wheatstone bridge circuit for optimal sensitivity. The connecting cable is then fed through the EVA and the back sheet to an external measurement device. Using this layout, we expect to be able to determine the cell strains directly while the module is loaded in the test stand and thus get the possibility to compare the measured strains to those obtained by Finite Element calculations.

VII. Conclusion

We identified three major influencing factors that stiffen a module and, hence help to reduce module deflection and thus cell stress. These are the glass thickness, the frame stiffness, and the embedment depth of the laminate in the frame. The deflections and stresses of the module depend strongly on the stiffness behaviour of EVA. But also with valid material properties of EVA it is inevitable for a realistic simulation of the module deformation by Finite Element analysis, to include

the frame behaviour in the model and to find a boundary condition that is a well suited approximation to the real bonding situation. Finally, one should be aware of the fact that a small variation of the Finite Element boundary conditions may result in a disproportionate larger variation of stresses, especially when either frame or laminate or both are weak.

We further expect that we can measure the cell strains by applying strain gauge rosette micro-strain sensors to the cells and can calibrate the calculation model with it.

ACKNOWLEDGEMENTS

This work was conducted as part of the K-Project *IPOT* within the Austrian R&D programme *COMET - Competence Centres for Excellent Technologies*. Funding by the Federal Ministries of Transport, Innovation, and Technology (BMVIT), of Economics and Labour (BMWA) and the Provinces of Carinthia and Styria, managed on their behalf by the Austrian Research Promotion Agency (FFG), is gratefully acknowledged.

REFERENCES

[1] M. A. Hopcroft, W. D. Nix, and T. W. Kenny. "What is the Young's Modulus of Silicon?", *J. Microelectromechanical Systems*, **19, 2**, pp. 229-238, 2010.

[2] U. Eitner, M. Pander, S. Kajari-Schröder, M. Köntges, and H. Altenbach. "Thermomechanics of PV Modules including the Viscoelasticity of EVA", Paper *26th European Photovoltaic Solar Energy Conference and Exhibition Proceedings*, pp. 3267-3269, Hamburg, Germany, Sept. 5--9, 2011.

[3] http://www.kern.de/cgi-bin/riweta.cgi?nr=1451&lng=1 Ethylen/Vinylacetat (E/VA) / Mechanische Eigenschaften